KSCE Journal of Civil Engineering (2020) 24(3):816-825
DOI 10.1007/s12205-020-0603-3

pISSN 1226-7988, eISSN 1976-3808
www.springer.com/12205

Nuclear Power Engineering

Nonlinear Finite Element Analysis of Prestressed Concrete Containment Vessel under Severe Accident Loads

Song Jin[a], **Zhongcheng Li**[b], **Tianyun Lan**[c], **Zhanfa Dong**[b], **and Jinxin Gong**[a]

[a]*State Key Laboratory of Costal and Offshore Engineering, Dalian University of Technology, Dalian 116024, China*
[b]*State Key Laboratory of Nuclear Power Safety Monitoring Technology and Equipment, China General Nuclear Power Corporation, Shenzhen 518029, China*
[c]*China Nuclear Power Design Co., Ltd., China General Nuclear Power Corporation, Shenzhen 518029, China*

ARTICLE HISTORY

Received 3 April 2019
Accepted 6 January 2020
Published Online 14 February 2020

KEYWORDS

Prestressed concrete containment vessel
Nonlinear finite element analysis
Pressure capacity
Thermal effects
Nonlinear displacement response

ABSTRACT

Prestressed concrete containment vessel act as a reliable leak tight barrier during the accident conditions. There is a growing demand to study nonlinear behavior of containment structure under severe accident loads in depth. This paper presents nonlinear finite element analysis of prsestressed concrete containment vessel under severe accident loads with consideration of material nonlinearity, penetrations, local reinforcement and temperature-dependent degradation characteristic of materials. To reflect the prestressing effects realistically, non-uniform distribution of effective prestressing along the tendon profile is explicitly considered and python scripts are developed to add the corresponding temperature drop value for each node of the prestressed tendons to ABAQUS input files automatically. Nonlinear finite element analysis for pressure only case and combined thermal and pressure case has been investigated in detail. Nonlinear finite element analysis results of the containment structure indicate that, thermal effects have negligible effect on pressure capacity of containment, considering the thermal effects, pressure capacity of containment decrease not more than 5% and margin of the containment still meets the requirements of not less than 2.5. The effect of temperature exhibit significantly influence on displacement response of containment structure, and the effect of temperature on the strain of liner and reinforcing steel is much greater than that on prestressed tendon. Thermal effects exhibit the greatest influence on nonlinear displacement response of the dome apex location and the least influence on the 33 m elevation.

1. Introduction

Containment structures in nuclear power plants play the critical role of providing the final barrier against the release of radioactive materials into the environment during the severe accidents (Spencer et al., 2006). External and internal events are considered in the design of the containment (IAEA, 1998). Fukushima nuclear accident happened in Japan highlighted the need for the robust design of concrete containments (IAEA, 2011). In recent decades, many experimental and numerical studies focused on pressure capacity of the containment structures had been conducted. Experimental studies include a 1:6 scale reinforced concrete containment and a 1:4 scale prestressed concrete containment at Sandia National Laboratories in America (Horschel, 1992; Hessheimer et al., 2003), MAEVA mock up in France (Kevorkian et al., 2005), 1:4 scaled model of inner containment structure in India (Singh, 2011). Because of the high cost of containment model test, numerical analysis of the containment structures is inevitable. Huang et al. (2017) conducted nonlinear finite element analysis of containment structure to evaluate the performance of the containment structure with consideration of time-dependent aging effects. Hu and Lin (2016) studied the pressure capacity and failure mode of the containment vessel using the finite element software ABAQUS with consideration of the long-term prestressing loss. Shokoohfar and Rahai (2016) performed nonlinear analysis of 1:4 containment model subjected to high pressure and temperature, anchorage details of the steel liner are explicitly considered. Zhang et al. (2014) evaluated structural integrity of the containment and the internal structures under steam explosion scenarios. Noh et al. (2008) studied the effects of high temperature

CORRESPONDENCE Jinxin Gong jinxingong@163.com State Key Laboratory of Costal and Offshore Engineering, Dalian University of Technology, Dalian 116024, China

and pressure on containment behavior based on the axisymmetric three-dimensional finite element model. Zhou et al. (2014) investigated nonlinear behavior of the containment under the utmost internal pressure coupled with loss of coolant accident temperature. Most studies mentioned above mainly focus on mechanical loading (such as gravity, prestressing and internal pressure) and thermal effects are ignored. Although there are some studies focus on thermal effects on containment structure, but effects of thermal loading has not been thoroughly studied. The leak proof boundary role of the containment is seriously threatened by loads under severe accident conditions. Severe accident loads should be considered specifically in the design of future containments (Amin et al., 1993). What's more, the influence of temperature on the containment nonlinear behavior had not been studied extensively. Last but not least, the study of International Standard Problem 48 on containment capacity shows that there are no consistent conclusions about the effect of temperature on the behavior of containment structure (Prinja and Curley, 2007). This paper presents nonlinear finite element analysis of prestressed concrete containment vessel under severe accident loads in depth. Results of this study can provide insights into the influence of thermal effects on nonlinear behavior of containment under severe accidents and it also can provide technical support for development of severe accident management guidelines (SAMG) in nuclear power plant.

2. Finite Element Model of Containment

2.1 Containment Geometry Model

Prestressed concrete containment in this study is composed of dome, cylinder wall, ring beam, prestressed tendon system and base slab. The interior surface of the containment is arranged with the 6mm-thick steel liner to provide leak tightness. The overall height of the containment is 71.7 m from bottom of the base slab to the dome apex location. The inner radius and outer radius of the containment is 22.5 m and 23.7 m, respectively. The thickness of dome and base slab is 1.0 m and 4.0 m, respectively. Details of the containment are displayed in Fig. 1. Fig. 2 shows the relative location of major penetrations on the cylinder wall.

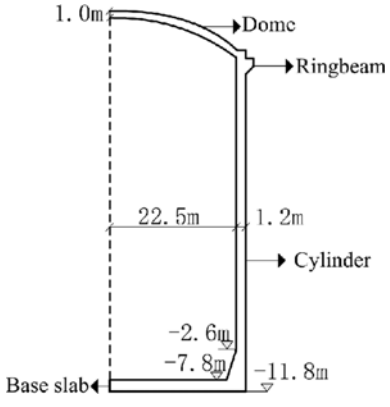

Fig. 1. Cross Section View of the Containment

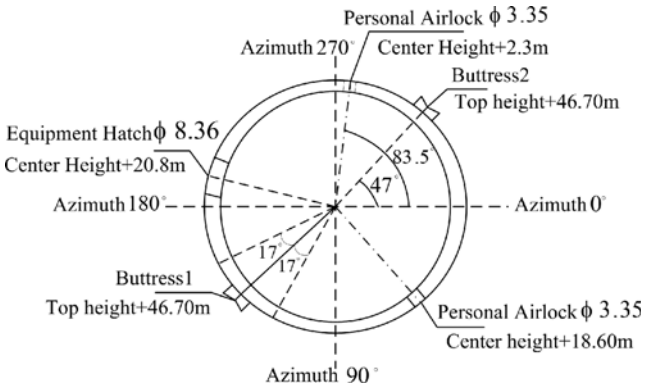

Fig. 2. Penetrations of Cylinder Wall

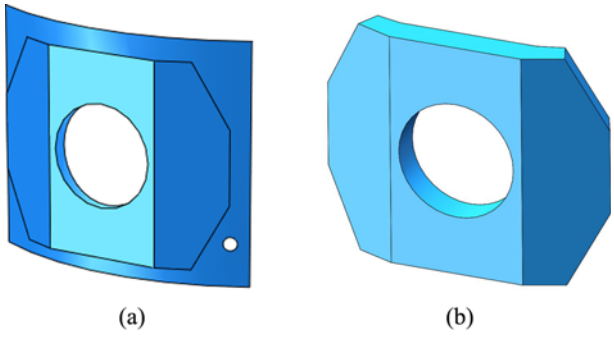

Fig. 3. Details around Penetration: (a) Local Reinforcement, (b) Local Thicken Area

Prestressed tendon system in this containment is consisted of hoop tendons, vertical tendons and U-shaped tendons. Hoop tendons are post-tensioned on both ends and anchored at buttresses. Vertical tendons are tensioned at upper end and vertical tendons are anchored at the tendon gallery and on top of the ring beam. One end of U-shaped tendons is anchored at the tendon gallery, and the other end of U-shaped tendons is anchored on the ring beam. Design pressure of this containment is 0.42 MPa (relative pressure). To prevent early failure around major penetrations additional rebars with complex shape and local thicken area are provided around penetrations. Details around penetrations are explicitly considered in this study (see Fig. 3).

2.2 Material Properties and Constitution

Five kinds of materials are used in the containment i.e., concrete, reinforcing steel, steel liner, prestressed tendon, penetration assemblies. Mechanical and thermal properties of concrete are listed in Table 1. Mechanical properties steel materials are listed in Table 2. Thermal conductivity and specific heat capacity of concrete are set equal to 1.4 W/(m·°C) and 879 J/(kg·°C) according to relevant literature (Hessheimer and Dameron, 2006). Thermal conductivity, specific heat and thermal expansion coefficient of steel liner set equals to 45 W/(m·°C) and 500 J/(kg·°C), respectively. A value of 1.2×10^{-5}/°C have been used as the thermal expansion coefficient for steel liner. It should be noted that some steel materials cannot be used in subsequent thermal conductivity

Table 1. Material Characteristic of Concrete

f_c / MPa	f_t / MPa	E_c / MPa	υ_c	γ_c / kg/m^3	α_c / °C	λ_c (J/m·°C·s)	C_c (J/kg·°C)
50	4.07	36,000	0.2	2,500	0.00001	1.4	879

Note: f_c is ultimate compressive strength of the concrete; f_t is tensile strength of the concrete; E_c is Young's modulus of the concrete; υ_c is the Poisson's ratio of the concrete; γ_c is density of the concrete; α_c is thermal expansion coefficient of the concrete; λ_c is the specific heat of the concrete; C_c is the thermal conductivity of the concrete.

Table 2. Material Mechanical Characteristic of Steel Materials

Material Name	Steel Grade	Density (kg/m^3)	Young's Modulus (MPa)	Poisson's ratio	Yield strength (MPa)
Reinforcing steel	HRB500	7850	200,000	0.3	435
Steel liner	P265GH	7850	200,000	0.3	299.5
Prestressed tendon	1860	7800	195,000	0.3	1653
Penetration assemblies	P265GH	7850	200,000	0.3	299.5

analysis, so relevant thermal characteristics are not given in this study and properties of material are determined with respected to relevant literature (Jin et al., 2019).

2.2.1 Concrete

Concrete damaged plasticity model provided by software ABAQUS is used to simulated nonlinear behavior of concrete. Main failure mechanisms in concrete damaged plasticity model are tensile cracking and compressive crushing for concrete material in software ABAQUS. Nonlinear behavior of concrete behavior can be expressed as:

$$\sigma_t = (1-d_t)E_0\left(\varepsilon_t - \tilde{\varepsilon}_t^{pl}\right) \tag{1}$$

$$\sigma_c = (1-d_c)E_0\left(\varepsilon_c - \tilde{\varepsilon}_c^{pl}\right) \tag{2}$$

where σ_t and σ_c are the tensile stress and compressive stress of concrete; d_t, d_c is the tensile damage factor and compressive damage factor of concrete; E_0 is the initial elastic modulus of concrete ε_t and ε_c are the tensile strain and compressive strain of concrete; $\tilde{\varepsilon}_t^{pl}$ and $\tilde{\varepsilon}_c^{pl}$ are equivalent tensile plastic strain and equivalent compressive plastic strain. Damage factor d_t, d_c can be calculated using the following formula:

$$d_c = 1 - \frac{\sigma_{cu}/E_0}{\tilde{\varepsilon}_c^{pl}(1/b_c - 1) + \sigma_{cu}/E_0} \tag{3}$$

$$d_t = 1 - \frac{\sigma_{tu}/E_0}{\tilde{\varepsilon}_t^{pl}(1/b_t - 1) + \sigma_{tu}/E_0} \tag{4}$$

where σ_{tu} and σ_{cu} are the tensile stress and compressive stress at unloading point. Compressive and tensile damage parameter is set equal to 0.7 and 0.1, respectively, according to Birtel and Mark (2006). Compressive constitution of concrete is determined according to Eurocode2 Part 1-1 (EN1992-1-1, 2010a). To simulate the tension stiffening behavior of the containment structure, linear strain softening behavior is used and the ultimate tensile strain ε_{tu} is set equal to 0.0023 according to relevant literature (Alhanaeea et al., 2018). Uniaxial constitutive relationship of concrete is shown in Fig. 4.

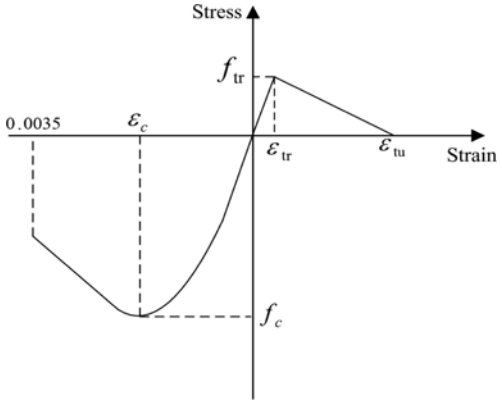

Fig. 4. Uniaxial Stress-Strain Curve of Concrete

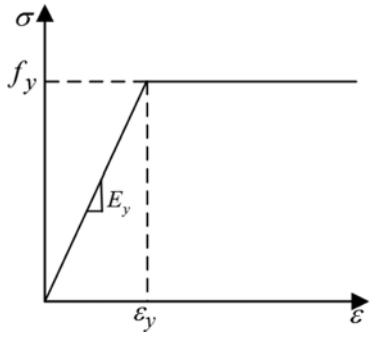

Fig. 5. Constitution of Steel Materials

2.2.2 Steel Materials

Elastic perfectly plastic model is used for steel liner, penetration assemblies and reinforcing steel and prestressed tendon according to Zhou et al. (2018). Stress-strain relationship of steel materials is illustrated in Fig. 5.

2.3 Finite Element Mesh

Figure 6 demonstrates mesh of the containment structure. Concrete part is modeled using 8-noded brick elements with reduced integration scheme (C3D8R), steel liner and penetration assemblies are modeled using reduced integrated 4-noded general shell

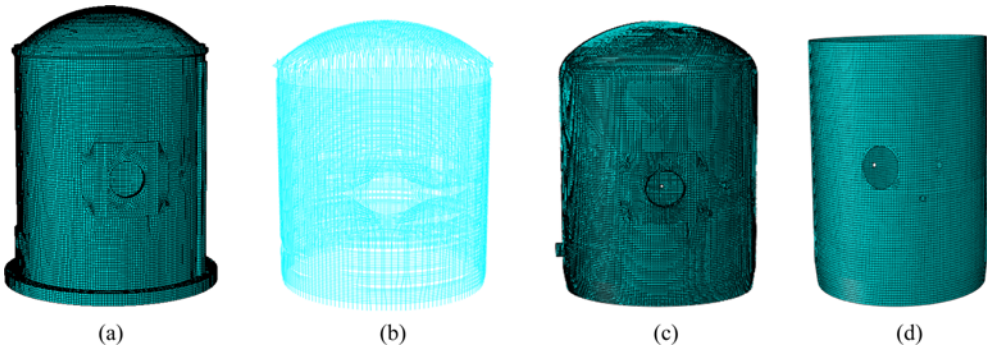

Fig. 6. Constitution of Steel Materials: (a) Concrete, (b) Prestressed Tendon, (c) Steel Liner, (d) Reinforing Steel

Table 3. Element Information Used in FE Analysis

Part name	Element types	Quantities of element
Concrete	C3D8R and C3D6	190,314
Steel liner and penetration assemblies	S4R and S3	108,286
Prestressed tendon	T3D2	53,104
Reinforcing steel	SFM3D4 and SFM3D3	41,044

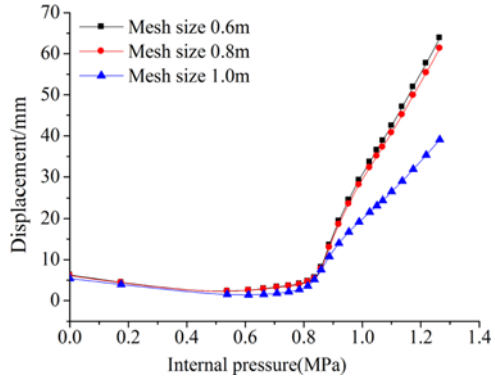

Fig. 7. Displacement versus Internal Pressure for Mid-Height of Cylindrical Wall with Different Mesh Size

elements (S4R). Surface elements SFM3D4 and SFM3D3 is used to simulate rebar layers. Table 3 summarizes types and quantities of element for the containment FE model. Mesh sensitivity analysis is needed because of the cracking characteristics of concrete (Tong et al., 2018). Fig. 7 depicts the displacement for mid-height location of containment versus internal pressure with different mesh size. According to Fig. 7, the calculated results meshed with 0.6 m and 0.8 m is close to each other. However, the calculated results with mesh size 1.0 m show significant difference between the results with mesh size 0.6 m and 0.8 m. Finite element analysis in this study is performed with mesh size 0.8 m.

2.4 Boundary Conditions, Constraints and Prestressing Simulation Method

All degrees of freedom on the bottom surface of the containment structure are constrained and all steel materials are embedded into the concrete solid elements using embedding technique in ABAQUS and the sliding effects are neglected (ABAQUS-6.12, 2012b). Prestressing loss in prestressed tendons can classified be into two types i.e., non time-dependent losses and time-dependent losses. non time-dependent losses of prestressing including friction loss, anchorage slip losses and elastic shortening of the concrete. Time-dependent losses include shrinkage and creep of concrete and relaxation of presstressed tendons. Friction and anchorage slip losses are dependent on tendons geometry and long-term losses are dependent on material properties (Tavakkoli et al., 2017). Reverse friction loss method is used to determine the anchorage slip loss. Prestressing loss can be calculated with respect to Eurocode2 Part 1-1 (EN1992-1-1, 2010a). It should be noted that long term losses are calculated at the end of plant service life. Prestressing effect can be simulated with either initial stress method or decreasing temperature approach, Decreasing temperature approach is adopted to simulate prestressing effects and the corresponding temperature drop value can be determined as following:

$$\Delta T = \sigma_{\text{pe}} / (\alpha E_p) \tag{5}$$

where σ_{pe} is effective prestressing after considering prestressing loss; E_p is the Young's modulus of prestressed tendon; α is the themal expansion coefficient of prestressed tendon.

To reflect the prestressing effects realistically, non-uniform distribution of effective prestressing along the tendon profile is explicitly considered in this study. Python scripts are developed to determine the corresponding temperature drop value for each node of the prestressed tendons.

It should be mentioned that, decreasing temperature for each prestressed tendons has been transformed into the format in ABAQUS INP file, and it has been added directly to the keywords of INP file of containment finite element model through Python script in the corresponding data item (following the* initial conditions type = temperature).

3. Nonlinear Finite Element Analysis of the Containment

3.1 Failure Criteria

For cylindrical prestressed concrete containments, the pressure

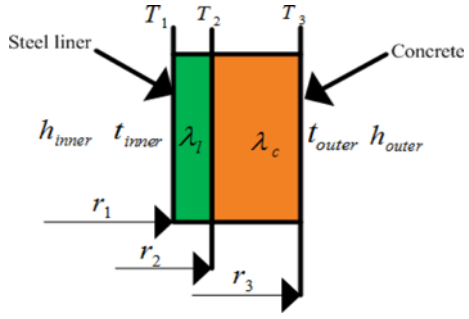

Fig. 8. Schematic Sketch of Heat Transfer Analysis

capacity of the containment structure can be determined based on strain based failure criteria illustrated in USNRC RG1.216 (U. S. Nuclear Regulatory Commission, 2010).

3.2 Heat Transfer Analysis

To obtain the temperature distribution of the containment, heat transfer is carried out. In heat transfer analysis step, concrete solid elements are meshed with heat transfer element DC3D8 and DC3D6, steel liner and penetration assemblies are meshed using element DS4 and DS3, prestressed tendons are modeled using DC1D2 elements. Heat transfer process can be subdivided into four parts, which includes inner surface convection between the internal steam and the steel liner, conduction of the steel liner, conduction of concrete and conduction between concrete outer surface and ambient. The heat convection coefficient between the outer surface of the containment and ambient is set equal to 16W/(m^2·°C) and inner surface between the ambient is set equal to 8W/(m^2·°C) according to relevant code (RCC-CW, 2015). Under loss of coolant accident condition, temperature boundary condition at inner surface is assumed that T_3 = 150°C and outer surface of concrete is assumed to be the ambient temperature as T_1 = 20°C. Schematic sketch of heat transfer analysis is illustrated in Fig. 8.

3.3 Semi-Coupled Thermal-Stress Analysis

To gain insight into thermal effects on nonlinear behavior of the containment, combined thermal and pressure case are investigated in detail. It should be noted that, reinforcing steel is simulated with *rebar layer command in software ABAQUS, this type of element cannot be used in fully coupled thermal-stress analysis (ABAQUS-6.12, 2012a). Sequentially coupled thermal-stress analysis is adopted in this study. Sequentially semi-coupled thermal-stress analysis technique in ABAQUS is used for combined thermal and pressure case. In sequentially coupled thermal-stress analysis, nodal temperatures of the containment FE model are read from heat transfer analysis and are applied at each increment as a steady state temperature. To reflect the material behavior under elevated temperature realistically, temperature-dependent degradation characteristic of materials are explicitly considered in this study. Temperature-dependent degradation characteristics for materials are determined according to Eurocode Part 1-2 (EN1992-1-1, 2010b).

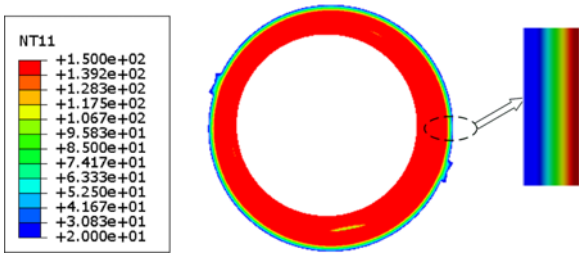

Fig. 9. Temperature Distribution of Containment Wall Thickness

3.4 Nonlinear Finite Element Analysis Results

3.4.1 Heat Transfer Analysis Results

Figur 9 shows temperature distribution through containment wall thickness direction. It can be seen that the temperature field shows a band-like distribution along the wall thickness of the containment, which gradually decreases from the inside surface of containment to the outside surface of the containment. The inner surface of containment temperature is 150°C and the outer surface of containment is 20°C.

3.4.2 Displacement Distribution of Containment under Different Pressure Levels

Figure 10 presents displacement distribution of containment for pressure only case and combined thermal pressure case at the pressure of 0.63 MPa. Maximum displacement and displacement

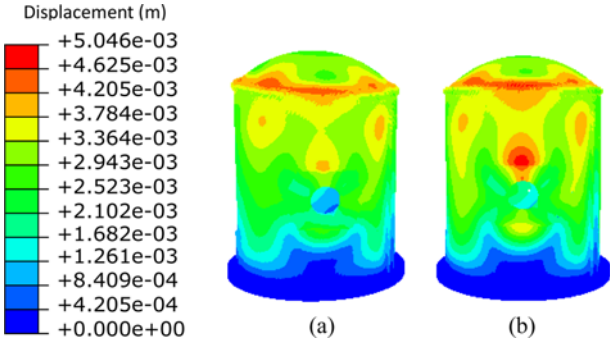

Fig. 10. Displacement Distribution of Containment at 0.63 MPa: (a) Pressure Only Case, (b) Combined Thermal and Pressure Case

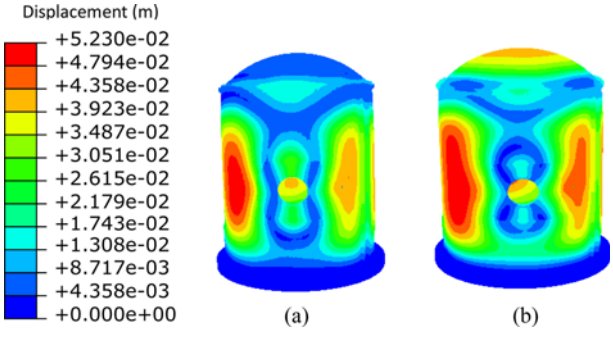

Fig. 11. Displacement Distribution of Containment at 1.05 MPa: (a) Pressure Only Case, (b) Combined Thermal and Pressure Case

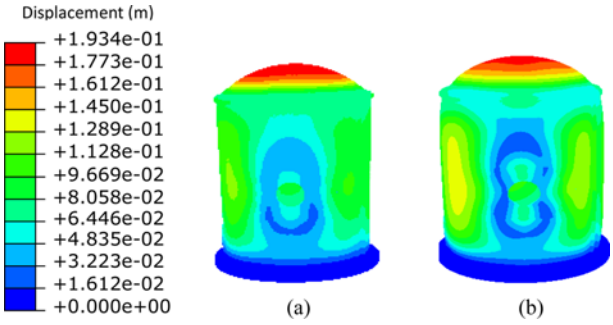

Fig. 12. Displacement Distribution of Containment at 1.47 MPa: (a) Pressure Only Case, (b) Combined Thermal and Pressure Case

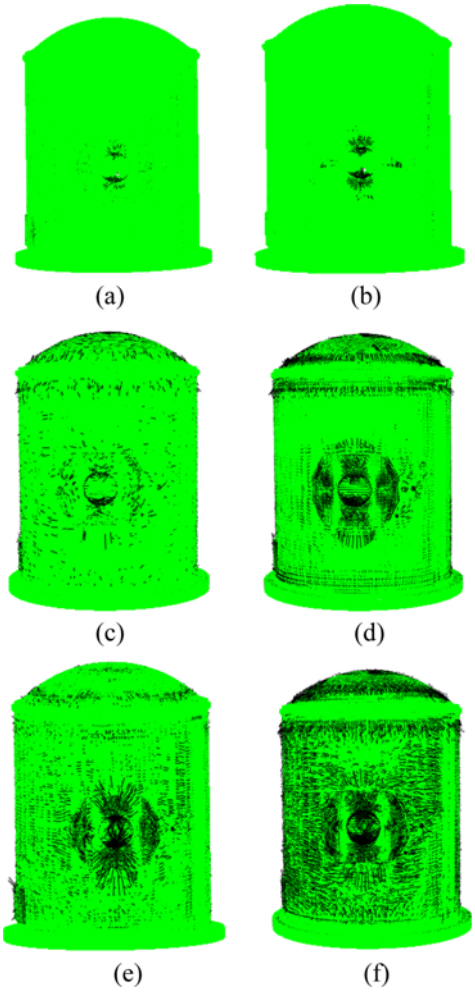

Fig. 13. Crack Pattern of Containment Structure under Different Internal Pressure Levels: (a) Pressure Only Case at 0.63 MPa, (b) Combined Thermal and Pressure Case at 0.63 MPa, (c) Pressure Only Case at 1.05 MPa, (d) Combined Thermal and Pressure Case at 1.05 MPa, (e) Pressure Only Case at 1.05 MPa, (f) Combined Thermal and Pressure Case at 1.05 MPa

distribution of the containment for pressure only case and combined thermal pressure case is almost the same.

Figure 11 demonstrates displacement distribution of the containment for pressure only case and combined thermal and

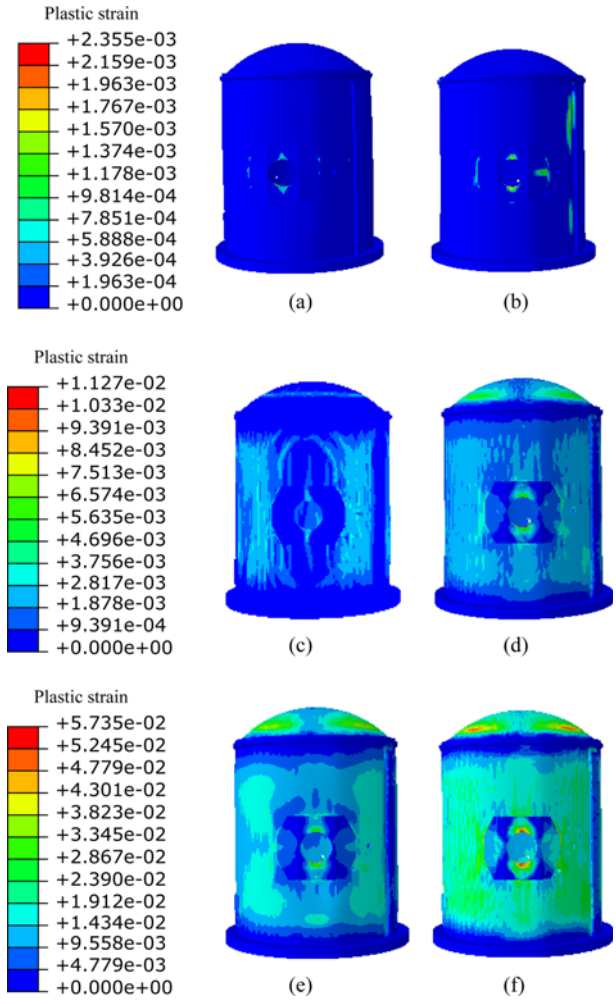

Fig. 14. Plastic Strain Distribution of Containment Structure under Different Internal Pressure Levels: (a) Pressure Only Case at 0.63 MPa, (b) Combined Thermal and Pressure Case at 0.63 MPa, (c) Pressure Only Case at 1.05 MPa, (d) Combined Thermal and Pressure Case at 1.05 MPa, (e) Pressure Only Case at 1.47 MPa, (f) Combined Thermal and Pressure Case at 1.47 MPa

pressure case at the pressure of 1.05 MPa. The difference between the maximum displacement of the containment for pressure only case and combined thermal and pressure case become obvious.

Figure 12 depicts displacement distribution of the containment for pressure only case and combined thermal and pressure at the pressure of 1.47 MPa. Redistribution of the displacement appears and the maximum displacement of the containment appears on dome apex location of the containment. Maximum displacement of containment is 157.7 mm and 193.4 mm for pressure only case and combined thermal and pressure, respectively.

3.4.3 Crack and Plastic Strain Distribution of Containment under Different Pressure Levels

Figures 13 and 14 illustrate the crack pattern and plastic strain distribution of containment under different pressure levels. When the internal pressure load is small, the effect of temperature on the cracking status and plastic strain of containment is negligible.

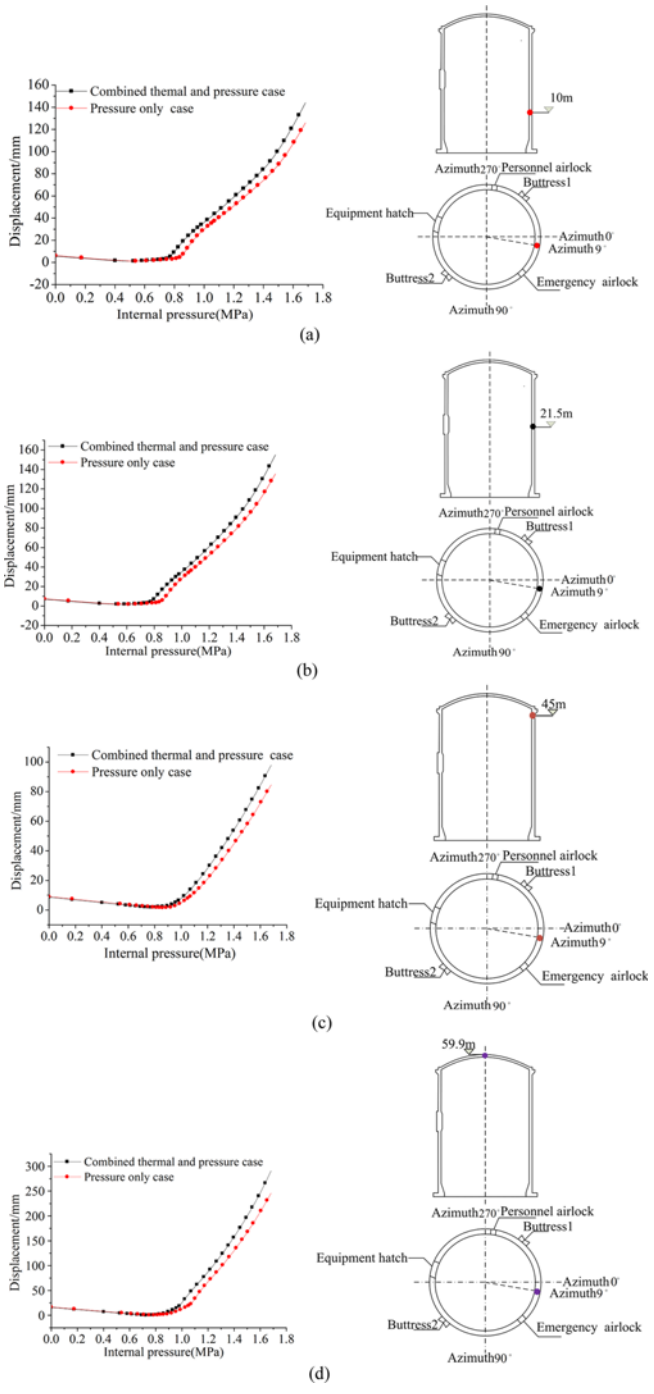

Fig. 15. Displacement versus Internal Pressure of Containment at Different Elevations: (a) Elevation of 10 m, (b) Elevation of 21.5 m (mid-height of cylinder wall), (c) Elevation of 45.0 m, (d) Elevation of 55.9 m (dome apex location)

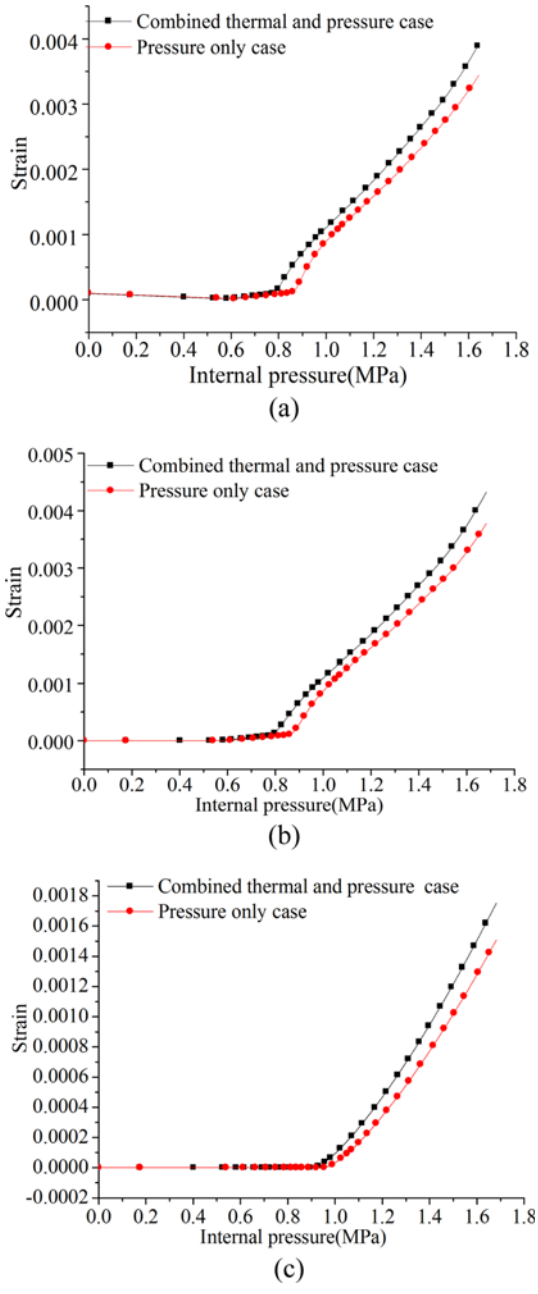

Fig. 16. Strain versus Pressure Response at Mid-Height of Containment: (a) Steel Liner, (b) Reinforcing Steel, (c) Prestressed Tendon

When the internal pressure load goes up to higher levels, thermal effect significantly affects cracking status and plastic strain of containment structure.

3.4.4 Displacement of Containment at Different Elevations

To evaluate thermal effects on the nonlinear behavior of containment, displacement versus internal pressure curves at different elevations of the containment under pressure only case and combined thermal and pressure case are shown in Fig. 15. It can be seen that for elevations less than 45 m, when the internal pressure less than 0.8 MPa, the displacement for pressure only case and combined thermal and pressure case almost the same and difference of displacement for pressure only case and combined thermal and pressure case become obvious when the internal pressure goes beyond 0.8 MPa. For elevations larger than 45 m, displacement of containment for pressure only case and combined thermal and pressure case show obvious difference when the internal pressure goes up beyond 0.9 MPa.

3.4.5 Strain of Materials at Mid-Height of the Cylinder Wall

Figure 16 demonstrates the strain versus pressure curves at mid-height of the cylindrical wall. For internal pressure level lower than 0.8 MPa, strain of steel liner and reinforcing steel for pressure only case and combined thermal and pressure case is very small and their difference is negligible. After internal pressure exceeds 0.8 MPa, strain of steel liner and reinforcing steel for combined thermal and pressure case is much higher than that of pressure only case. As for prestressed tendon, the influence of thermal effects on the strain of prestressed tendon can be neglected when the internal pressure is lower than 1.0 MPa and thermal effects show significant influence on the strain of prestressed tendon when the internal pressure goes up beyond 1.0 MPa.

4. Evaluation of Thermal Effects on Containment Behavior

4.1 Thermal Effects on Pressure Capacity of Containment

Pressure capacity of the containment for pressure only case and combined thermal and pressure case are determined with respect to the above mentioned failure criteria and the corresponding pressure capacity of the containment are listed in Table 4. It can be seen that, when thermal effects are considered, pressure capacity of containment based on liner failure criteria decreased about 5%, pressure capacity of containment based on reinforcing steel failure criteria decreased about 4% and pressure capacity of containment based on prestressed tendon failure criteria decreased about 5%. When considering thermal effects, margins between design pressure of the containment based on liner failure criteria decreases from 3.24 to 3.07, margins between design pressure of the containment based on reinforcing steel failure criteria decreases from 3.81 to 3.64 and margins between the design pressure of the containment based on prestressed tendon failure criteria decreases from 3.93 to 3.74. In general, pressure capacity of the containment structure decrease by no more than 5% when thermal effects are included and margin of the containment still meets the requirements of not less than 2.5.

Table 4. Comparison of Pressure Capacity of the Containment (MPa)

Failure criteria	Pressure only case	Combined thermal and pressure cases
Liner	1.36	1.29
Reinforcing steel	1.60	1.53
Prestressed tendon	1.65	1.57

4.2 Thermal Effects on Displacement Response of Containment

4.2.1 Comparison of Displacement for Two Kinds of Loading Cases

Table 5 presents displacement at different elevations of the containment under pressure only and pressure combined thermal loading cases. When the internal pressure reaches 1.05 MPa, thermal effects exhibit the greatest influence on the nonlinear displacement response of the containment at different elevations. Thermal effects exhibit the greatest influence on nonlinear displacement response at the dome apex location (elevation 59.9 m) and the least influence on the 33 m elevation. The effect of temperature on the displacement response of containment structure is related to the internal pressure level. Considering thermal effect, displacement of containment structure increased about 15.5% for pressure level reach 0.63 MPa, 42.3% for pressure level reach 1.05 MPa, 15.4% for pressure level reach 1.47 MPa. It should be noted that, since the range of displacement variation for each elevation of the containment is different, the average increase rate is used in this study. In general, nonlinear response of the containment is strongly affected by thermal effect during the severe accidents, because concrete will develop cracks under thermal gradients between the internal wall and external wall of the containment structure.

5. Conclusions

Nonlinear finite element analysis of prestressed concrete containment vessel under severe accident loading had been performed based on detailed three dimensional finite element model of containment structure. Material nonlinearity, non-uniform distribution of effective prestressing and temperature-dependant material degradation are considered. Nonlinear response and ultimate pressure capacity for pressure only case and combined thermal and pressure case had been studied in depth. The following conclusion can be obtained:

1. In general, thermal effects have negligible impact on pressure capacity of containment, considering the thermal effects, while exert significantly influence on the displacement response of containment structure.
2. When the internal pressure level is lower, the effect of

Table 5. Comparison of Displacement at Different Elevations for Two Kinds of Loading Cases (mm)

Pressure levels	Pressure only case					Combined thermal and pressure case				
	10 m	21.5 m	33 m	45 m	59.9 m	10 m	21.5 m	33 m	45 m	59.9 m
0.63 MPa	1.7	1.9	2.3	2.8	2.1	1.9	2.0	2.4	3.3	2.9
1.05 MPa	35.4	34.1	32.6	8.4	19.4	41.7	41.2	35.7	12.1	42.6
1.47 MPa	83.6	90.7	82.5	53.9	155.8	95.8	104.0	89.3	64.4	187.2

temperature on the strain of liner, reinforcing steel and prestressed tendon is small. With the increase of pressure level, the influence of temperature on strain of liner, reinforcing steel and prestressed tendon increased. In general, the effect of temperature on the strain of liner and reinforcing steel is much greater than that on prestressed tendon.

3. The effect of temperature is related to the location of containment and internal pressure level. Thermal effects exhibit the greatest influence nonlinear displacement response at the dome apex location and the least influence on the 33 m elevation of the containment. Thermal effects exhibit the greatest influence on the nonlinear displacement response when the internal pressure level reaches 1.05 MPa.

Acknowledgements

This research was supported by Grant K-A2018-502 from scientific research program of China General Nuclear Power Corporation (CGN). The authors would also like to acknowledge the anonymous reviewers whose critical comments and useful suggestions have been valuable with improving the quality of the manuscript.

ORCID

Song Jin https://orcid.org/0000-0002-5244-3511

References

ABAQUS-6.12 (2012a) ABAQUS analysis user's manual. ABAQUS 6.12, Dassault Systèmes Simulia Corp., Providence, RI, USA

ABAQUS-6.12 (2012b) User documentation-theory manual. ABAQUS 6.12, Dassault Systems Simulia, Corp., Providence, RI, USA

Alhanaeea S, Yongsun YS, Schifferc A (2018) Ultimate pressure capacity of nuclear reactor containment building under unaged and aged conditions. *Nuclear Engineering and Design* 335:128-139, DOI: 10.1016/j.nucengdes.2018.05.017

Amin M, Eberhardt AC, Erler BA (1993) Design considerations for concrete containments under severe accident loads. *Nuclear Engineering and Design* 145(3):331-339, DOI: 10.1016/0029-5493(93)90243-3

Birtel V, Mark P (2006) Parameterised finite element modelling of RC beam shear failure. Proceedings of the 19th annual international ABAQUS users conference, May 23-25, Boston, MA, USA, 95-108

EN1992-1-1:2010 (2010a) Design of concrete structures-Part 1-1: General rules and rules for buildings. EN1992-1-1:2010, European Committee for Standardization, Brussels, Belgium

EN1992-1-1:2010 (2010b) Design of concrete structures-Part 1-2: General rules-Structural fire design. EN1992-1-1:2010, European Committee for Standardization, Brussels, Belgium

Hessheimer MF, Dameron RA (2006) Containment integrity research at sandia national laboratories: An overview. NUREG/CR-6906, Sandia National Laboratories, Washington, DC, USA

Hessheimer MF, Klamerus EW, Lambert LD, Rightley GS (2003) Over pressurization test of a 1:4-scale prestressed concrete containment vessel model. Technical Report No.NU-REG/CR-6810, SAND2003-0840P, Nuclear Regulatory Commission, Washington, DC, USA

Horschel DS (1992) Experimental results from pressure testing of a 1:6 scale nuclear power plant containment. Technical Report No. NU-REG/CR-5121, SAND88-0906, Nuclear Regulatory Commission, Washington, DC, USA

Hu HT, Lin JX (2016) Ultimate analysis of PWR prestressed concrete containment under long-term prestressing loss. *Annals of Nuclear Energy* 87:500-510, DOI: 10.1016/j.anucene.2015.10.005

Huang X, Kwon O-S, Bentz E, Tcherner J (2017) Evaluation of CANDU NPP containment structure subjected to aging and internal pressure increase. *Nuclear Engineering and Design* 314:82-92, DOI: 10.1016/j.nucengdes.2017.01.013

IAEA (1998) Assessment and management of ageing of major nuclear power plant components important to safety: Concrete containment building. IAEA-TECDOC-1025, International Atomic Energy Agency, Vienna, Austria

IAEA (2011) International fact finding expert mission of the Fukushima Dai-Ichi NPP accident following the great east Japan earthquake and tsunami. Technical Report, International Atomic Energy Agency, Vienna, Austria

Jin S, Li ZC, Lan TY, Gong JX (2019) Fragility analysis of prestressed concrete containment under severe accident condition. *Annals of Nuclear Energy* 131:242-256, DOI: 10.1016/j.anucene.2019.03.034

Kevorkian S, Heinfling G, Courtois A (2005) Prediction of a containment vessel mock-up cracking during over design pressure test. Transactions of the 18th international conference on structural mechanics in reactor technology (SMiRT18), August 7-12, Beijing, China

Noh SH, Moon IH, Lee JB, Kim JH (2008) Analysis of prestressed concrete containment vessel under severe accident loading. *Nuclear Engineering and Technology* 40(1):77-86, DOI: 10.5516/NET.2008.40.1.077

Prinja NK, Curley JA (2007) Effect of thermal loading on containment capacity. Transactions of the 19th international conference on structural mechanics in reactor technology (SMiRT 19), August 12-17,Toronto, Canada

RCC-CW (2015) Rules for design and construction of PWR nuclear civil works. French Association for Design, Construction and In-Service Inspection Rules for Nuclear Island Components, Paris, France

Shokoohfar A, Rahai A (2016) Nonlinear analysis of pre-stressed concrete containment vessel (PCCV) using the damage plasticity model. *Nuclear Engineering and Design* 298:41-50, DOI: 10.1016/j.nucengdes.2015.12.019

Singh RK (2011) Post-test preliminary report on international round robin analysis for ultimate load capacity assessment of BARCOM test model. Reactor Safety Division, BARC, Mumbai, India

Spencer BW, Petti JP, Kunsman DM (2006) Risk-informed assessment of degraded containment vessels. NUREG/CR-6920, Sandia National Laboratories,Washington, DC, USA

Tavakkoli I, Kianoush MR, Abrishami H, Han X (2017) Finite element modelling of a nuclear containment structure subjected to high internal pressure. *International Journal of Pressure Vessels and Piping* 153:59-69, DOI: 10.1016/j.ijpvp.2017.05.004

Tong L, Zhou X, Cao X (2018) Ultimate pressure bearing capacity analysis for the prestressed concrete containment. *Annals of Nuclear Energy* 121:582-593, DOI: 10.1016/j.anucene.2018.08.020

U.S. Nuclear Regulatory Commission (2010) Containment structural integrity evaluation for internal pressure loadings above design basis pressure. Regulatory Guide 1.216, U.S. Nuclear Regulatory Commission, Rockville, MD, USA

Zhang CY, Chen P, Zhang JH, Lin JM, Liu YL, Zhang SS, Wang B (2014) Evaluation of the structural integrity of the CPR1000PWR

containment under steam explosion accidents. *Nuclear Engineering and Design* 278:632-643, DOI: 10.1016/j.nucengdes.2014.08.019

Zhou L, Li JB, Zhon H, Lin G, Li ZH (2018) Fragility comparison analysis of CPR1000 PWR containment subjected to internal pressure. *Nuclear Engineering and Design* 330:250-264, DOI: 10.1016/j.nucengdes.2018.02.005

Zhou Z, Wu C, Meng SP, Wu J (2014) Mechanical analysis for prestressed concrete containment vessels under loss of coolant accident. *Compute Concrete* 14(2):127-143, DOI: 10.12989/cac.2014.14.2.127